Springer Proceedings in Earth and Environmental Sciences

Joshapat Tetuko Sri Sumantyo
Pakhrur Razi *Editors*

Advances in Geoscience and Remote Sensing Technology

Proceedings of the 2nd IC-GEOREST (October 26–27, 2024, Padang, Indonesia)

Springer

Springer Proceedings in Earth and Environmental Sciences

The series Springer Proceedings in Earth and Environmental Sciences publishes proceedings from scholarly meetings and workshops on all topics related to Environmental and Earth Sciences and related sciences. This series constitutes a comprehensive up-to-date source of reference on a field or subfield of relevance in Earth and Environmental Sciences. In addition to an overall evaluation of the interest, scientific quality, and timeliness of each proposal at the hands of the publisher, individual contributions are all refereed to the high quality standards of leading journals in the field. Thus, this series provides the research community with well-edited, authoritative reports on developments in the most exciting areas of environmental sciences, earth sciences and related fields.

Joshapat Tetuko Sri Sumantyo · Pakhrur Razi
Editors

Advances in Geoscience and Remote Sensing Technology

Proceedings of the 2nd IC-GEOREST, October 26–27, 2024, Padang, Indonesia

Springer

Editors
Joshapat Tetuko Sri Sumantyo
Center for Environmental Remote Sensing,
Chiba University
Chiba, Chiba, Japan

Pakhrur Razi
Center of Disaster Monitoring and Earth
Observation, Universitas Negeri Padang
Padang, Indonesia

ISSN 2524-342X ISSN 2524-3438 (electronic)
Springer Proceedings in Earth and Environmental Sciences
ISBN 978-981-95-3074-8 ISBN 978-981-95-3075-5 (eBook)
https://doi.org/10.1007/978-981-95-3075-5

This Springer imprint is published by the registered company Springer Nature Singapore Pte Ltd.
The registered company address is: 152 Beach Road, #21-01/04 Gateway East, Singapore 189721, Singapore

Preface

The 2nd International Conference on Geoscience, Remote Sensing, and Technology (IC-GEOREST 2024), to be held on October 26–27, 2024, in Padang, Indonesia, marks a significant milestone in the field of geoscience and remote sensing. As we convene in this dynamic location, we aim to foster global collaboration and knowledge exchange among researchers, industry professionals, and policymakers to address pressing challenges and explore innovative solutions in the rapidly evolving fields of geoscience and remote sensing technology.

The importance of geoscience in understanding the Earth's systems and environment has never been more critical. As we face climate change, natural disasters, urbanization, and resource management issues, the role of remote sensing technologies has become indispensable. Remote sensing allows us to collect data from various platforms, including satellites, drones, and ground-based sensors, enabling real-time monitoring, analysis, and decision-making on a global scale. By leveraging these advanced technologies, we gain insights into phenomena ranging from weather patterns to deforestation, sea-level rise to urban expansion.

IC-GEOREST 2024 serves as a platform to showcase cutting-edge research, best practices, and applications in geoscience and remote sensing. Over the two-day conference, we will delve into a range of topics, including but not limited to satellite imagery analysis, climate change monitoring, environmental impact assessment, disaster management, geospatial data processing, and the integration of artificial intelligence with geospatial technologies. These areas are critical to addressing both local and global challenges, especially in regions like Southeast Asia, where geographical diversity and vulnerability to environmental hazards are significant concerns.

This conference is not only an opportunity for academic and professional exchange but also a call to action for interdisciplinary collaboration. In a world where environmental challenges transcend national boundaries, the need for cooperative efforts across disciplines—such as geology, environmental science, data science, and engineering—has never been more urgent. By uniting experts from various sectors, IC-GEOREST 2024 aims to contribute to the development of sustainable and technologically advanced solutions to ensure a resilient and prosperous future.

The conference also highlights Indonesia's strategic role in the global geoscience and remote sensing landscape. As one of the world's most biodiverse and geographically complex nations, Indonesia stands at the forefront of addressing challenges related to disaster resilience, environmental protection, and resource management. The local context of Padang, with its unique geological setting and vulnerability to natural disasters such as earthquakes and tsunamis, provides a perfect backdrop for meaningful discussions on how remote sensing technologies can be utilized to mitigate risks and enhance disaster preparedness.

We are excited to bring together leading experts, practitioners, and emerging researchers to engage in meaningful discussions, share knowledge, and form partnerships that will shape the future of geoscience and remote sensing. We hope that IC-GEOREST 2024 will spark innovative ideas and contribute to the global efforts in advancing geospatial technologies for a sustainable planet.

Welcome to Padang, Indonesia, and to an inspiring and enriching conference experience.

Adree Octova
General Chair of 2nd IC-GEOREST 2024

Organizing Committee IC-GEOREST 2024

Advisory

Josaphat Tetuko Sri Sumantyo	Center of Remote Sensing, Chiba University, Japan
Yohandri	Universitas Negeri Padang, Indonesia

General Chair

Adree Octova	Center of Disaster Monitoring and Earth Observation, Universitas Negeri Padang, Indonesia

Co-chair

Pakhrur Razi	Physics Department, Universitas Negeri Padang, Indonesia

Secretary

Najmi Asyifa	Universitas Negeri Padang, Indonesia
Alfi Nasution	Universitas Negeri Padang, Indonesia

General Treasurer

Febrian Hidayat	Universitas Negeri Padang, Indonesia

International Scientific Board Member

Gaofeng Ren	Wuhan University of Technology, China
Chistopher D. Elvidge	Colorado School of Mines, Colorado, US
Ang Kiang Long	INTI International University, Malaysia
Husnul Kausarian	Universitas Islam Riau, Indonesia

Mirza Muhammad Waqar	Contec. Ltd., Korea
Jamrud Aminuddi	Sudirman University, Indonesia
Prof. Yohandri	Universitas Negeri Padang, Indonesia
Yuta Izumi	Muroran Institute of Technology, Japan
Ming Yam Chua	Xiamen University, Malaysia
Hein Yang	Contec. Ltd., Korea
Sarun Apichontrakul	Khon Kaen University, Thailand
Katia Urata	European Space Agency
Refky Adi Nata	Wuhan University of Technology, China

Local Organizing Committee Coordinator

Riko Maiyudi	Universitas Negeri Padang
Yoszi Mingsi Anaperta	Universitas Negeri Padang
Febrian Syukra	Universitas Negeri Padang
Dian Adhetya Arif	Universitas Negeri Padang
Zulhendra Hendra	Universitas Negeri Padang

Local Organizing Committee Member

Miftahurrahman Alpaba
Muthia Azizah
Nabila Zahra
Agung Wahyudi
Muhammad Iqbal
Febrian Hidayat

Contents

Land Deformation of West Sulawesi Due to the Earthquake in 2021–2022 Based on Sentinel-1A Data Processing Using the DinSAR Methods

Jamrud Aminuddin[1(✉)], Tika Ayunda Vita[1], Ilham Alimuddin[2], Pakhrur Razi[3], Indra Riyanto[4], Asif Awaludin[5], Albert Sulaiman[5], Joko Widodo[6], Babag Purbantoro[6], Vicca Karolinoerita[6], Destika Cahyana[7], Rachmat Abdul Gani[7], and Rufaidah Qonita Muslim[7]

[1] Faculty of Mathematics and Natural Sciences, Department of Physics, Universitas Jenderal Soedirman, Jl. dr. Suparno 61, Purwokerto 53122, Indonesia
jamrud.aminuddin@unsoed.ac.id
[2] Faculty of Engineering, Department of Geological Engineering, Universitas Hasanuddin, Jl. Poros Malino Km 6, Sungguminasa 92171, Indonesia
[3] Center of Disaster Monitoring and Earth Observation, Physics Department, Universitas Negeri Padang, Padang 25131, Indonesia
[4] Center for Environmental Studies, Universitas Budi Luhur, Jl. Cileduk Raya 99, Jakarta Selatan 12260, Indonesia
[5] Research Center for Climate and Atmospheric, National Research and Innovation Agency, Jl. Sangkuriang, Dago, Kecamatan Coblong, Bandung 40135, Indonesia
[6] Research Center for Geoinformatics, National Research and Innovation Agency, Jl. Sangkuriang, Dago, Kecamatan Coblong, Bandung 40135, Indonesia
[7] Research Center for Food Crops, National Research and Innovation Agency, Kawasan Sains dan Teknologi (KST), Dr. (H.C) Ir. H. Soekarno Jl. Raya, Jakarta-Bogor KM. 46, Cibinong, Bogor, West Java 16915, Indonesia

Abstract. One of the natural phenomena that often occurs in Indonesia is earthquakes, one of which is in West Sulawesi Province. Land conditions in the province experienced many changes after the earthquake in 2021 and 2022. Considering that the analysis of Sentinel-1A image data uses the DInSAR (Differential Interferometry Synthetic Aperture Radar) method in research in several ground conditions, which can describe in detail the ground deformation, then in this research, further exploration will be carried out regarding this method to analyze post-earthquake soil conditions in West Sulawesi in 2021 and 2022. This research generally aims to monitor soil deformation where the earthquake occurred using Sentinel-1A satellite imagery processed using the Differential Interferometry Synthetic Aperture Radar (DInSAR) method. Deformation observations using four pairs of Sentinel-1A images with data acquisition in 2020–2022 Level-1 SLC (Single Look Complex) with dual polarization (VV: Vertical-Vertical and VH: Vertical-Horizontal) and Interferometry Wide acquisition mode (IW). Based on the results of data processing that has been carried out, it is known that the land deformation that occurred before the earthquake occurred was a rise in land level of 0.002 meters and a decrease in land level of −0.078 meters. At the time of the earthquake, the

J. T. S. Sumantyo and P. Razi (Eds.): IC-GEOREST 2024, SPEES, pp. 495–514, 2026.
https://doi.org/10.1007/978-981-95-3075-5_39

land level dropped by −0.370 meters, and the land level rose by 0.670 meters. So, the average deformation due to an earthquake is a rise in land level of 0.130–0.360 meters and a decrease in land level of −0.100 to −0.550 meters.

Keywords: Deformation · DInSAR · Earthquake · Land · Sentinel

1 Introduction

The earth's surface is a dynamic object, where the forces that occur around the earth's surface will influence the shape of the earth. Land deformation is one of the phenomena that occurs due to the earth's surface dynamics [1]. Land deformation also causes several problems, such as damage to building structures, increased seawater absorption areas, and increased flood areas. This phenomenon can be caused by several processes, such as sediment placement, and non-natural ones, such as groundwater extraction, petroleum, gas, underground mining, and earthquakes [2]. One of the natural phenomena that often occurs in Indonesia is earthquakes. Indonesia's territory causes it is located above the Ring of Fire [3]. The movement of the three large plates flanking Indonesia gave rise to a series of volcanoes and significant tectonic activity [4, 5]. The Indonesian region also consists of islands with different seismic circumstances and conditions and varying levels of risk in each region. This condition causes earthquakes to become the most frequently experienced natural disaster, with relatively significant losses depending on each area's vulnerability level [6].

Sulawesi Island is one of Indonesia's islands with a high earthquake potential. West Sulawesi Province, which covers an area of approximately 16,796.19 km^2, is an administrative region formed on October 5, 2004, based on Law No. 26 of 2004. Figure 1 shows a map of the Republic of Indonesia archipelago with the official source BIG (Geospatial Information Agency). Several sources indicate that several West Sulawesi Province areas are still rebuilding after experiencing earthquakes in 2021 and 2022. The 2021 West Sulawesi earthquake was a 6.2 Mw land earthquake that hit the west coast of Sulawesi Island, Indonesia, on January 15, 2021, at 02.28 CIST (Central Indonesian Standard Time). The earthquake's epicenter was 7 km northeast of Majene, West Sulawesi, with a depth of 10 km. During the recovery process, in 2022, Mamuju Regency, as the capital of West Sulawesi province, experienced another earthquake on June 8, 2022, at 13.32 WITA with the epicenter of the earthquake located at sea, to be precise 26 km west of Tapalang, Mamuju, West Sulawesi. The hypocenter of the earthquake occurred at a depth of 10 km.

The **earthquake** that occurred in Mamuju City was a shallow earthquake due to the activity of the Mamuju-Majene fault with a thrust fault mechanism. After the initial earthquake, the aftershocks had a frequency that was repeated enough to cause severe damage to the buildings above them. The primary mechanism for faults is divided into block changes (deformation) before an earthquake occurs and block deformation after an earthquake occurs [7, 8].

As previously explained, Land deformation due to the earthquake will be analyzed using remote sensing technology. The remote sensing systems currently being developed are satellites based on optical remote sensing (ORS) and synthetic aperture radar (SAR).

Fig. 1. West Sulawesi Province's location on the Republic of Indonesia archipelago map is marked with a circle (Source: Geospatial Information Agency)

Both systems have proven to recognize objects on the Earth's surface after processing digital data from a satellite sensor system. Several methods have been developed in the spatial domain that detect deformation and land cover recorded on satellite images. It is supported by the quality of satellite imagery with a reasonably high spatial resolution that has reached the order of centimeters, especially for SAR systems. However, the temporal resolution is still low on the daily order [9–13]. Optical satellites with geostationary orbit systems have a high temporal resolution that has reached the order of minutes. However, the spatial resolution is still shallow, on the order of kilometers. This type of satellite is usually designed to record atmospheric dynamics [14–18].

Observations of land deformation can be carried out by utilizing Sentinel-1 data as a SAR (synthetic aperture radar) sensor installed on a space satellite at an altitude of more than 400 km from the earth's surface. This satellite can observe single polarization (HH and VV) and double polarization (HV and VH). Sentinel-1 (Level 1.0) provides observations with 4 modes [13, 19, 20]. SAR data processing, especially using the Permanent Scatterer Interferometric (PS-InSAR) method, has proven capable of analyzing patterns and values of land surface deformation due to the manifestation of mud volcanoes in the East Java Basin region. Long-term soil deformation using the Quasi-Persistent Scatterer (Q-PS) technique has also been applied in Kelok Sembilan, West Sumatra Province [12]. The most important thing in utilizing Sentinel-1 data, which uses C-band SAR is deformation that reaches accuracy in millimeters [21, 22]. The latest research uses Sentinel-1 satellite imagery data to map, evaluate, and explain the causes of land subsidence in the Nile River Delta, Egypt. The InSAR method is applied with the support of GPS data, tides, land use maps, and vegetation indices [23]. Considering that the analysis of Sentinel-1 image data using the InSAR and PS-InSAR methods in previous research was able to describe in detail ground deformation, in this study, further exploration will be carried out regarding these methods to analyze post-earthquake soil conditions in West Sulawesi.

2 Method

The area that will be reviewed is the earthquake's location in West Sulawesi Province. The earthquake occurred with a magnitude of 6.2 Mw, with the epicenter being 27 km southeast of Mamuju City or at a latitude of 2.97°S and longitude 118.99°E with a depth of 10 km. Figure 2 shows the earthquake's location from https://vsi.esdm.go.id/index.php. This source shows that on January 14, 2021, at 14:35 CIST, West Sulawesi, its surroundings were shaken by an earthquake of M 5.9. This earthquake was followed by a more giant earthquake (6.2 Mw) that hit this area again 13 hours later. The Meteorological, Climate, and Geophysics Agency of Indonesia stated that the first earthquake had its epicenter at 118.89°E and 2.9°S. In contrast, the second earthquake was centered at 118.94°E and 2.98°S with an epicenter depth of 18 km. This study generally aims to monitor land deformation in the area of Mamuju regency-West Sulawesi Province-Indonesia, using Sentinel-1A satellite imagery processed using the Differential Interferometry Synthetic Aperture Radar (DInSAR) method. Figure 3 shows the Sentinel 1A data processing procedure.

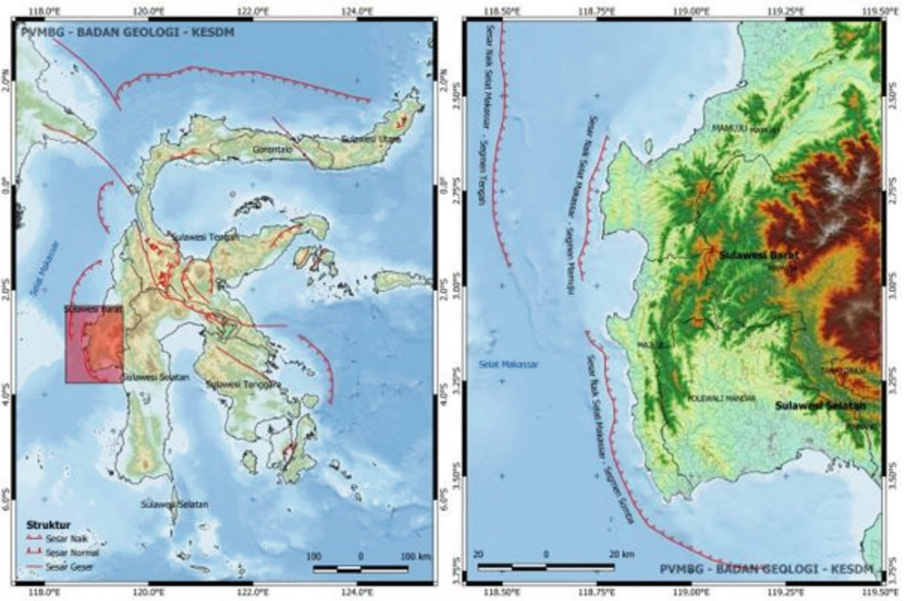

Fig. 2. Sulawesi Island and West Sulawesi Province's (Source: Center for Volcano, Minerals, and Geological disasters).

The Sentinel-1A satellite has a 12-day interval for image acquisition and a spatial resolution of up to 20 m. Therefore, this allows for improved monitoring of natural events such as earthquakes, volcanoes, and landslides. The amount of deformation can be analyzed based on the results of Sentinel-1A image data processing with Interferometric Wide (IW) acquisition mode and a spatial resolution of 5 by 20 meters (Single Look).

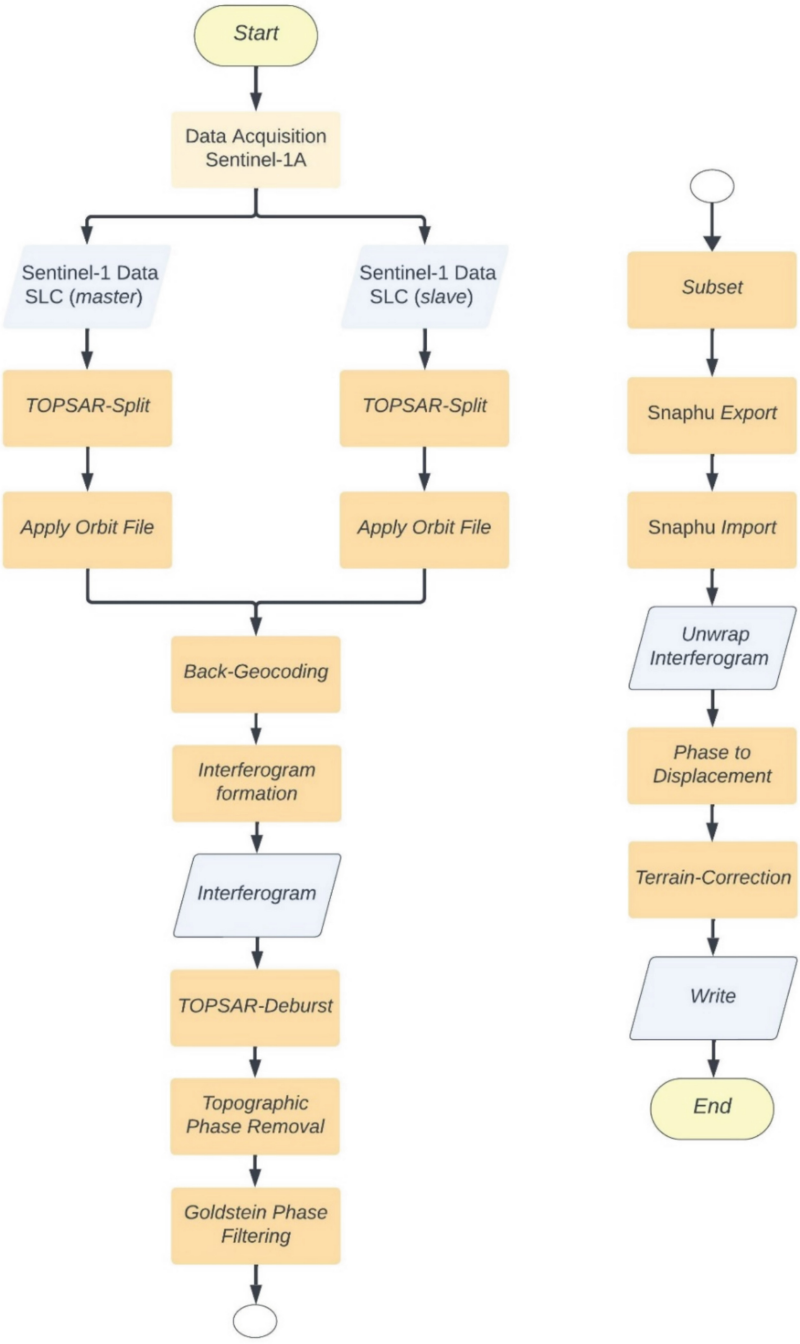

Fig. 3. Flowchart of Sentinel 1A data processing.

The satellite image data acquired were satellite images in 2020 before the earthquake, satellite image data in 2021 immediately after the earthquake, and satellite image data in 2022 after the earthquake occurred over a relatively long period. Sentinel-1A satellite image data is obtained through the official ESA database, which is then processed and can be visualized via Google Earth software. This method was developed from Ref. [24–26]. The acquisition methods in this analysis, shown in Fig. 2, originated from https://scihub.copernicus.eu/dhus/odata/v1/Products (Fig. 4).

Fig. 4. Data acquisition on the Sentinel-1A satellite, Source: https://scihub.copernicus.eu/dhus/odata/v1/Products.

SAR (Synthetic Aperture Radar) interferograms are generated based on precise sensor orbits, time information, and topography of surface areas, for example, from DEMs. This step assumes that an accurate DEM (Digital Elevation Model) is available that, when sampled at SAR resolution, allows for efficient topographic removal and spectral shift filtering. The interferogram phase (ϕ) can be estimated by calculating for each target P in the plane (azimuth, slant range), where the difference in sensor illumination range to reach the target for both satellites uses the equation

$$\phi\left(\overrightarrow{P}\right) = \frac{4\pi}{\lambda}\left(r_M\left(\overrightarrow{P}\right) - r_S\left(\overrightarrow{P}\right)\right) \approx \frac{4\pi B_n}{\lambda r_0}\Delta r\left(\overrightarrow{P}\right) \quad (1)$$

B_n is the perpendicular baseline, and r is the distance from the satellite to the target.

The SAR interferogram provides a usable unwrapped phase field. This phase can be subtracted from the final SAR interferogram result to remove known topography, thereby providing a differential interferogram to monitor changes. The following equation offers a pixel-to-pixel mapping map from the master image to the slave image, which will be used for image co-registration in the following equation,

$$\Delta r\left(\overrightarrow{P}\right) = \frac{4\pi}{\lambda}\left(r_M\left(\overrightarrow{P}\right) - r_S\left(\overrightarrow{P}\right)\right) \tag{2}$$

Information on $\phi\left(\overrightarrow{P}\right)$ can be used to provide optimal spectral shift filtering [27].

The co-registering step is a primary step in creating an interferogram. It ensures that each surface target contributes to the same pixels (slant range, azimuth) in the master and slave images. In the ideal case of perfectly parallel orbits and aligned acquisition, co-registering is indispensable to replace different geometries due to different viewing angles (parallax effect) [28]. Co-registering leverages image statistics to align the two products at sub-pixel accuracy. TOPSAR Split is applied to image data to select the bursts required for analysis. Using orbit files containing information regarding satellite positions during SAR data acquisition is also needed. Sentinel-1 provides a restructured Precise Orbit Determination (POD) and Precise Orbit Ephemerides (POE) orbit files for each image data. The POE file covers approximately 28 hours and contains orbital state vectors at 10-second intervals. The files produced are one per day and sent within 20 days after data acquisition [29].

The Co-registering maps can be written as polynomials capable of estimating pixel-to-pixel shifts, assuming targets on the Earth's surface are ellipsoidal. On Synthetic Aperture Radar satellites, including the Sentinel-1 satellite, the sensor speed and attitude are so stable that the master-slave deformation of the entire frame (100 × 100 km) can be well estimated by the following polynomial

$$r_S = a.r_M^2 + b.r_M + c.a_M + d \tag{3}$$

$$a_S = e.r_M^2 + f.r_M + g.a_M + h \tag{4}$$

Here r_M and a_M are the range and azimuth coordinates of the master image, respectively. The r_S and a_S are the range and azimuth coordinates of the slave image that must be evaluated. The coefficients in Eqs. and represent the transformations illustrated in Fig. 5. The azimuth shift with coefficient (d) is due to the time difference along the orbit, and the range shift (h) is due to the baseline perpendicular component. The range stretching (b) is due to baseline variations with range and azimuth stretching (g) due to variations in Pulse Repetition Frequency (PRF) and satellite speed. Tilt range (c) and azimuth (f) estimate image rotation for small rotation angles. Two second-order terms (a and e) are required to process the long-range tile [30] (Fig. 5).

The interferometric phase of each SAR image pixel will depend only on the distance from the SAR satellite to the required target resolution cell. Thus, the calculated interferogram contains phase variations (ϕ) of several contributing factors, namely the flat earth phase ϕ_{flat} (curvature of the earth), the topographic phase ϕ_{DEM} (topographic surface of the earth), the atmospheric conditions ϕ_{atm} (humidity, temperature and pressure

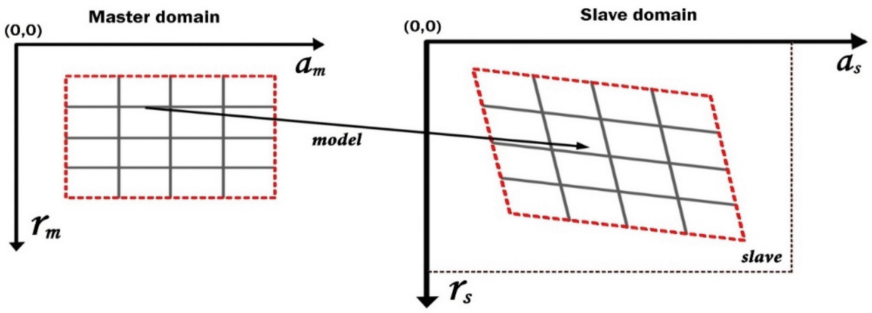

Fig. 5. Deformation model for registering slave images on the master reference grid.

changes between two acquisition), and other noise ϕ_{noise} (scattering changes, different viewing angles, and volume scattering), and finally, the surface deformation ϕ_{disp} that occurs between the two acquisitions. The whole interferometric phases are represented in linear summation as

$$\phi = \phi_{DEM} + \phi_{flat} + \phi_{atm} + \phi_{noise} \tag{5}$$

Once the surface reference point is identified, the travel path difference Δr variation that results in a shift from the reference resolution cell to another can be shown in Fig. 6. The influencing parameters are the perpendicular baseline (B_n), the target distance from the radar (R), and the displacement between resolution cells along the perpendicular to the slant range (q_s). The estimated Δr can be calculated using the following formula

$$\Delta \boldsymbol{r} = -\boldsymbol{2}\frac{\boldsymbol{B_n q_s}}{\boldsymbol{R}} \tag{6}$$

The interferometric phase variation $\Delta\boldsymbol{\phi}$ is proportional to Δr divided by the transmitted wavelength λ. For this reason, $\Delta\boldsymbol{\phi}$ can be expressed in

$$\Delta \boldsymbol{\phi} = \frac{\boldsymbol{2\pi}\,\Delta \boldsymbol{r}}{\boldsymbol{\lambda}} = \frac{\boldsymbol{4\pi}}{\boldsymbol{\lambda}}\,\frac{\boldsymbol{B_n q_s}}{\boldsymbol{R}} \tag{7}$$

The C-band of SAR from Sentinel-1A has a wavelength of approximately 5.5 cm. Furthermore, the interferometric phase variation can be divided into two contributions: the phase variation proportional to the height difference q between the point targets, referred to as the horizontal reference plane, and the phase variation proportional to the tilt range displacement s of the point targets. Therefore, $\Delta\boldsymbol{\phi}$ can be expressed in

$$\Delta\phi = \frac{4\pi}{\lambda}\,\frac{B_n q}{R\sin\theta} - \frac{4\pi}{\lambda}\,\frac{B_n q_s}{R\tan\theta} \tag{8}$$

Here, θ is the angle of incidence of the radiation [29].

The perpendicular baseline is known from precise orbital data, and the interferogram phase can be calculated by subtracting it from the interferometric phase. This step is called interferogram flattening, and a new phase is produced that is proportional to the field height [28]. When some scattering points on the ground slightly change their

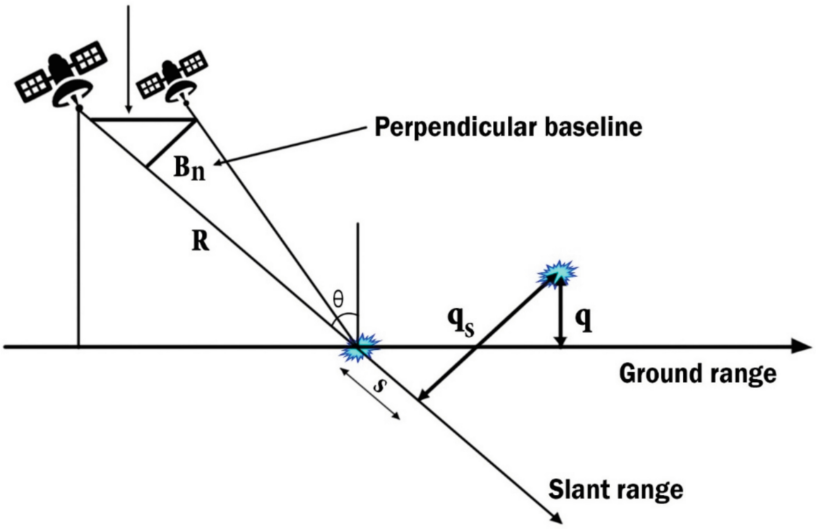

Fig. 6. Deformation model for registering slave images on the master reference grid.

relative position in the time interval between two SAR observations (e.g., if a subsidence, landslide, and earthquake occurs), then in such a case, the phase is separated from the baseline and appears in the interferometric phase as follows

$$\Delta\boldsymbol{\phi}_{\boldsymbol{d}} = \frac{\mathbf{4}\boldsymbol{\pi}}{\boldsymbol{\lambda}}\boldsymbol{d} \tag{9}$$

The d parameter indicates the relative scatter displacement projected in the slant range direction. The scatter means that after interferogram flattening, the interferometric phase contains height and motion contributions as

$$\Delta\phi - \frac{4\pi}{\lambda}\frac{B_n q}{R\sin\theta} - \frac{4\pi}{\lambda}d \tag{10}$$

The remaining phase variations can be attributed to changes in surface height between the two image acquisitions as

$$\phi_{disp} = \phi - \phi_{DEM} - \phi_{flat} \tag{11}$$

For the DInSAR method, the contribution from the earth's surface, ϕ_{flat}, and ϕ_{DEM} are considered the same for both image acquisitions, which can be removed from the interferogram.

When topographic phase removal is applied, the interferogram contains only variations of displacement, atmosphere, and noise. These variations are displayed on a rainbow scale ranging from $-\pi$ to $+\pi$. Patterns containing such variations in the interferogram are called fringes, representing a complete 2π cycle and appearing in the interferogram as random color cycles, where each cycle represents half the sensor wavelength. The relative ground motion between two points is then derived by calculating the fringe and

multiplying it by half the wavelength. The closer each fringe is, the greater the strain in the soil [30].

In addition to phase interferometry, coherence between the master image and the slave image is estimated to indicate the quality of phase information. Loss of coherence can result in poor interferometry, which may be caused by temporal decorrelation (over vegetation and water surfaces), geometric decorrelation (errors or inaccuracies in orbital metadata), and volumetric decorrelation (potential scattering mechanisms from multiple structures, such as complex vegetation or surfaces dry) [31]. Coherence is calculated as separate raster bands and indicates how similar each pixel is between the master and slave images on a scale from 0 to 1. Areas of high coherence will appear bright. Areas with poor coherence will be dark. In the image results, vegetation is shown to have low coherence, and buildings have very high coherence [32]. The reflectivity of the source is influenced by the contribution of noise, namely scene decorrelation noise, which can arise from changes in scattering properties between two acquisitions, from volumetric effects or baseline decorrelation. As a result, corrections need to be made to eliminate noise, which might reduce the interferogram quality.

The noise from temporal and geometric decorrelation, volume scattering, and other processing errors can corrupt interferometric phases. These processing steps aim to provide a co-registering phase to keep the primarily correlated contributions in the image. However, unrelated contributions (which behave like noise) are removed. In Fig. 7, changes in viewing angle indicate a frequency shift in reflectivity. The middle and bottom plots show the filters required to remove uncorrelated spectral contributions. This spectral shift has been calculated for a constant inclined field as

$$\Delta f = -f_0 \frac{B_n}{r_0 \tan(\theta - \alpha)} \tag{12}$$

The spectral shift Δf in Eq. 12 depends on the incidence angle (θ) and the slope of the field (α). Spectral shift filtering is usually assumed for the flat earth [30].

$$f_c(r) = \frac{f_{DC_M}(r) + f_{DC_S}(r)}{2} \tag{13}$$

Here, f_{DC} is the Doppler filter centroid with filter bandwidth that must maintain a standard bandwidth, as in the shaded area in the bottom plot of Fig. 8.

The interferometric phase in interferograms is still ambiguous and only known on a 2π scale. Therefore, to connect the interferometric phase with topographic height, the phase must first be opened (unwrapping phase). The ambiguity height is the height difference resulting in an interferometric phase change of 2π after smoothing the interferogram. Phase unwrapping resolves this ambiguity by integrating the phase differences between nearby pixels. After removing the integer height ambiguities, the phase variation between two points on the smoothed interferogram measures the height variation (Fig. 9). Thus, the unwrapped phase results are interpreted as the relative height or displacement between pixels of the two images [31, 33]. The quality and reliability of unwrapped phase results depend highly on input coherence. Reliable results become better when the field coherence is high. Although there is no definite threshold, to obtain good results, a minimum coherence of 0.3 is required [34].

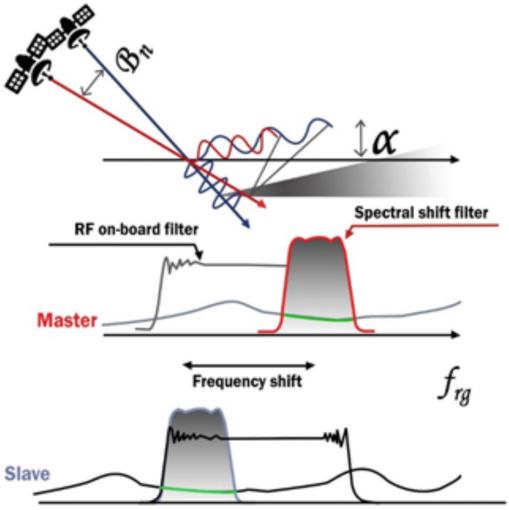

Fig. 7. Spectral shift in range.

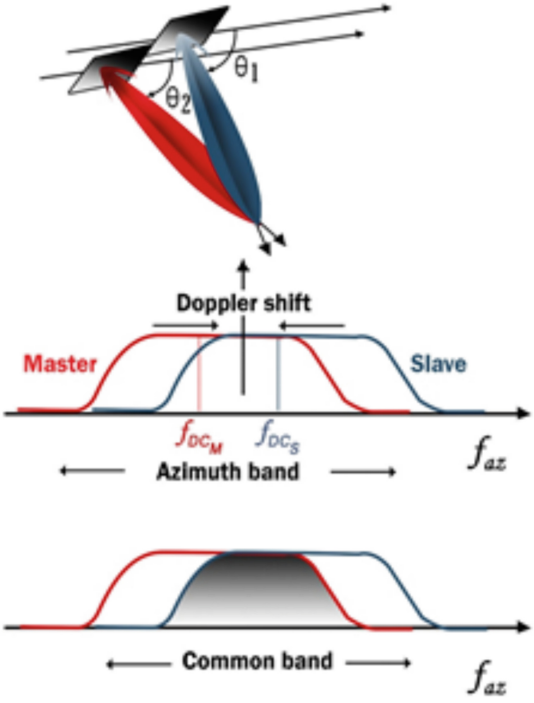

Fig. 8. Azimuth common band filtering.

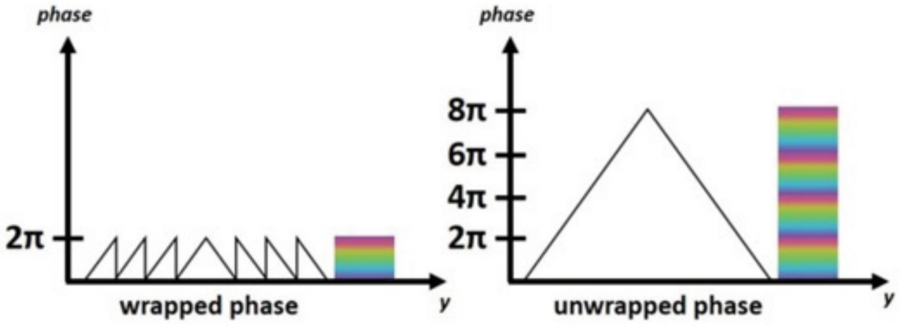

Fig. 9. Phase unwrapping principle.

The goal of phase unwrapping is to recover an integer number of n cycles that will be added to the wrapped phase (phi) so that an unambiguous phase value psi can finally be obtained for each image pixel as

$$\psi = \phi + 2\pi.n \tag{14}$$

Finally, to get the final result from a pair of images, apart from assuming there is no noise, it is necessary to estimate that the initial surface from which the data was taken is without interference. Then, phase to displacement needs to be applied to convert radian units to absolute displacement. This step translates the phase into surface changes along the meter's line of sight (LOS). LOS (line-of-sight) is the line between the sensor and the pixels. Thus, a positive value means a rise in the land surface (uplift), and a negative value represents a decrease in the land surface (subsidence). Phase to displacement has no parameters and is applied to the unwrapped phase in the last step. The resulting output looks similar to the unwrapped phase, but each pixel has a value indicating its displacement [35].

3 Results and Discussions

In this study, analysis of land deformation in the Mamuju Regency area was carried out by processing Sentinel 1A SAR image data. The data pairs used consist of 4 with acquisitions in 2020–2022 Level-1 SLC. The polarization involved is dual (VV: Vertical-Vertical and VH: Vertical-Horizontal) with Interferometric Wide (IW) acquisition mode, which is ultimately shown in Table 1. This table shows the data pair between serial numbers (1) and (2), which shows the ground deformation before the earthquake. In contrast, the data pair between serial numbers (2) and (3) represents the ground deformation several days after the earthquake. The data pair between sequence numbers (4) and (5) shows ground deformation a year after the earthquake. Furthermore, to determine the vital influence of the 2021 earthquake in the Mamuju Regency area, West Sulawesi Province, data with a serial number (1) was paired with data with a serial number (5). The data are originated from https://schub.copecus.eu/dhus/odata/v1/Products. The length of the perpendicular baseline and the time interval used in image pairs can cause temporal decorrelation. The

greater the length of the perpendicular baseline and the time interval, the greater the temporal decorrelation.

Table 1. Sentinel-1A image information of Mamuju Regency area, Source: https://scihub.copernicus.eu/dhus/odata/v1/Products.

No	Data name	Time Acquisition	Orbit	Direction
1	S1A IW SLC 1SDV 202009 04 T102649 20200904 T10271 6 034207 03F96C 4452	04 September 2020	34207	Descending
2	S1A IW SLC 1SDV 202012 21 T102648 20201221 T10271 5 035782 043035 6DA7	21 December 2020	35782	Descending
3	S1A IW SLC 1SDV 202101 26 T102647 20210126 T10271 4 036307 044286 0A33	26 January 2021	36307	Descending
4	S1A IW SLC 1SDV 202112 28 T102653 20211228 T10272 0 041207 04E5A0 3CD4	28 December 2021	41207	Descending
5	S1A IW SLC 1SDV 202202 02 T102652 20220202 T1027 8 041732 04F74B 346E	02 February 2022	41732	Descending

Table 2 shows that four different perpendicular baseline lengths were obtained for each IW pair from the four images used. From all image pairs, it was found that the most extended perpendicular baseline was 34.04 m, while the shortest perpendicular baseline was −17.48 m. This table shows that the time interval used for the image pairs for 21 December 2020–26 January 2021 and 28 December 2021–2 February 2022 is 36 days. In the image pair 4 September 2020–21 December 2020, it is 108 days; in the image pair 4 September 2020–2 February 2022, it is 516 days. The information is originated from https://scihub.copernicus.eu/dhus/odata/v1/Products.

To retrieve an interferogram, coherence values must be determined based on the data pairs, with the ranges between $0 \leq \gamma \geq 1$. The coherence value indicates the degree of similarity between image pairs and the quaity of the resulting interferogram. The greater the coherence value, the higher the image pair's identity level, and vice versa (Anjasmara & Muthmainnah, 2018). Based on the results of coherence calculations for data pairs in Tables 1 and 2 using the DInSAR method. The sample of image results is shown as an interferogram shape in Fig. 10.

Figure 11 shows the land condition before the earthquake occurred on 15 January 2021 using the image pair 4 September 2020–21 December 2020. The deformation occurred in land level rise (uplift) ranging from 0.002 to 0.212 meters, indicated by the light blue to red color range. The part of the interferogram dominated by color is evenly distributed in the interferogram area. Subsidence occurred at the top of the interferogram with a subsidence value of −0.078 meters, marked with a dark blue color range.

Table 2. The length baseline and time interval of Sentinel-1A image for Mamuju regency, Source: https://scihub.copernicus.eu/dhus/odata/v1/Products.

No	Pair of data	Length of baseline (m)	Time interval (days)
1	4 September 2020–21 December 2020	34.04	108
2	21 December 2020–26 January 2021	−21.37	36
3	28 December 2021–2 February 2022	−17.48	36
4	4 September 2020–2 February 2022	−67.28	516

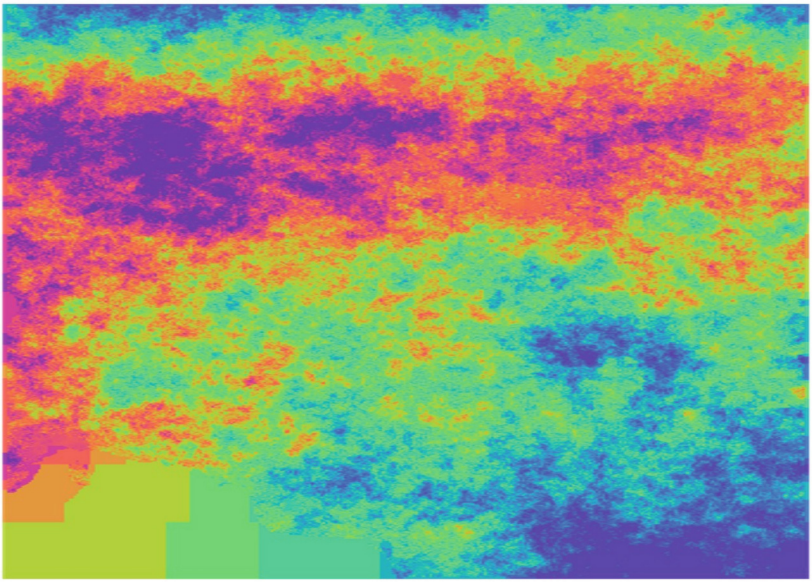

Fig. 10. The sample of image pair interferogram.

Figure 12 the image pair before the earthquake, namely the image pair 21 December 2020–26 January 2021, does not show any deformation in the form of land level rise (uplift). All interferograms show subsidence, where the most severe land subsidence occurs at the top of the interferogram, there is even subsidence of the land surface ranging from −0.190 to −0.010 meters, marked green to red. The land subsidence detected in this pair of ranges is likely to be the impact of the Mamuju earthquake on 15 January 2021.

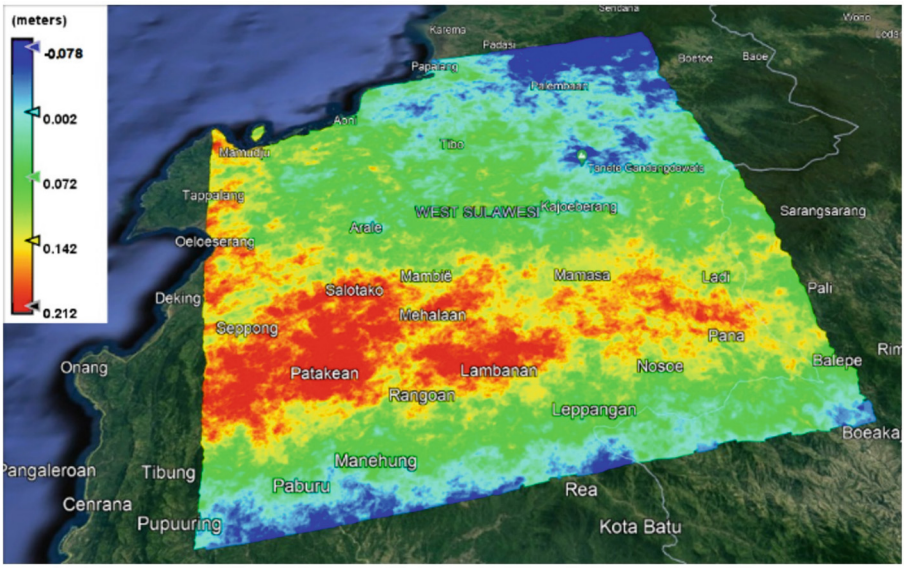

Fig. 11. The land conditions before the earthquake using image pairs of 4 September 2020–21 December 2020.

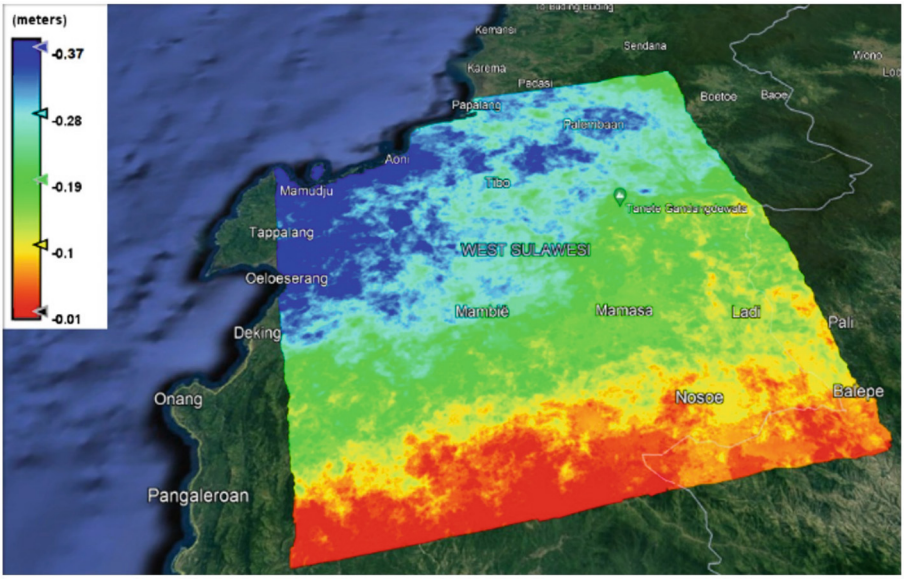

Fig. 12. The land deformation during the earthquake using image pairs of 21 December 2020–26 January 2021.

Figure 13 results from processing a pair of images in the same year after the earthquake, namely the image pair 28 December 2021–2 February 2022. This image does

not show any deformation in the form of subsidence. All interferograms show land level rise (uplift), where the most significant land level rise is marked in red to yellow, with values ranging from 0.052 to 0.640 meters. Then, the middle area of the interferogram, marked with bluish-to-green colors, shows the rise of the land level of 0.220 to 0.370 meters. The bottom of the interferogram saw the smallest rise in land level namely 0.070 meters, marked in dark blue. The rise in land level detected in the image pair in this range is likely due to rebuilding after the Mamuju earthquake.

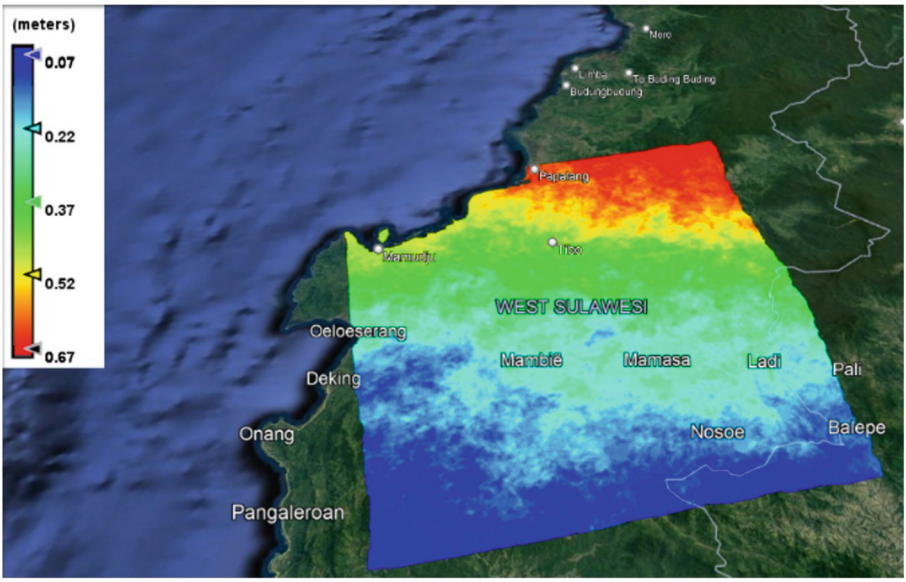

Fig. 13. The land deformation after the earthquake using image pairs of 28 December 2021–2 February 2022.

Figure 14 is a pair of images from 4 September 2020–2 February 2022 to test the total deformation long before and after the earthquake on 15 January 2021. The data processing results show that there is deformation in the form of land level rise (uplift) starting from 0.130 up to 0.360 meters, shown in the yellow to red color range. This image pair also detected subsidence with a value of −0.100 to −0.550 meters, marked with a color range of green to dark blue. The most significant deformation in Mamuju City was demonstrated during the Mamuju earthquake, which was marked by a considerable subsidence of the land surface. The Sentinel-1A SAR satellite can only detect surface areas, so geological conditions cannot be observed. Based on SAR data processing that has been carried out using the DInSAR method, a summary of land deformation in the Mamuju area can be seen in Table 3.

Research on earthquakes with a magnitude of Mw 6.2 in Mamuju and Majene, West Sulawesi Province, Indonesia, generated by active faults continuously extending to the Makassar Strait (Makassar Strait Thrust), was conducted using seismic data and the Global Positioning System (GPS). The study revealed that the primary earthquake, with

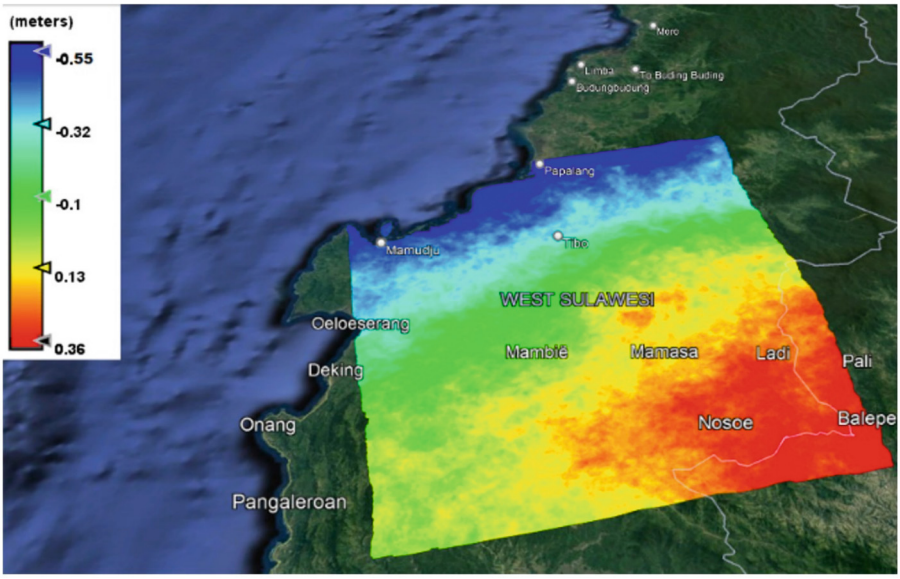

Fig. 14. The total land deformation before and after the earthquake using image pairs of 4 September 2020–2 February.

Table 3. The summary of land subsidence in Mamuju Regency area

No	Pair of data	Uplift (m)	Subsidence (m)
1	4 September 2020–21 December 2020	0.002 to 0.212	−0.078
2	21 December 2020–26 January 2021	–	−0,010 to −0,370
3	28 December 2021–2 February 2022	0.070 to 0.670	–
4	4 September 2020–2 February 2022	0.130 to 0.360	−0.100 to −0.550

a depth of 30 km, caused a segment of the MST to collapse and triggered a secondary fault structure [7, 35]. The responsible fault is the Mamuju fault [8]. This condition resulted in significant deformation in the Mamuju and Majene areas. Furthermore, the damage proxy map (derived from Sentinel-1 SAR scenes) in the Mamuju area, located more than 30 km from the epicenter, indicates an average probability of 0.9, evenly distributed. In contrast, the southern Mamuju and Majene areas, approximately 10 km from the epicenter, show an average probability of damage of 0.9, forming a linear distribution along the coastline. Land deformation after the earthquake indicates that deformation occurred predominantly in coastal areas (see Fig. 13). This result aligns with Ref [7] above with seismic, sentinel 1A SAR, and GPS approaches. As stated in Ref [7], the extent of the damage was caused by the Mamuju and Majene regions having a relatively higher crustal strain rate.

4 Conclusion

The occurrence of land deformation in the Mamuju area, West Sulawesi, Indonesia, due to the earthquake on 15 January 2021, has been analyzed using Sentinel-1A satellite image data. Employing the Differential Interferometry Synthetic Aperture Radar (DInSAR) method, the land eformation observed using four pairs of Sentinel-1A images with data acquisition in 2020–2022 Level-1 SLC (Single Look Complex) with dual polarization (VV: Vertical-Vertical and VH: Vertical-Horizontal) and Interferometric Wide acquisition mode (IW).

Based on the research that has been carried out, it can be concluded that the magnitude of land deformation that occurred in Mamuju City before the earthquake occurred had a land level rise of 0.002 to 0.212 meters and a land subsidence of −0.078 meters. The land surface dropped by −0.001 to −0.370 meters when the earthquake occurred. A year after the earthquake, the land level rose by 0.070 to 0.670 meters. So, the average deformation in Mamuju caused by the quake was a rise in land level of 0.130–0.360 meters and a decrease in land level of −0.100 to −0.550 meters.

References

1. Sophian, R.: Land subsidence in large cities on the north coast of Java (case study: Semarang city). Bulletin Scientific Contribution. **8**(1), 41–60 (2010)
2. Syafiudin, M., Chatterjee, R.: Potential use of satellite-based differential interferometric synthetic aperture radar (dinsar) technology for monitoring land success in the Bandung basin. GEOMATIKA. **15**(1) (2009)
3. Genrich, J., et al.: Accretion of the southern Banda arc to the Australian plate margin determined by global positioning system measurements. Tectonics. **15**(2), 288–295 (1996). https://doi.org/10.1029/95TC03850
4. Smyth, H., Hall, R., Nichols, J.: Cenozoic volcanic arc history of East Java, Indonesia: the stratigraphic record of eruptions on an active continental margin. In: Formation Applications Sedimentary Record Arc Collision Zones (2008). https://doi.org/10.1130/2008.2436(10)
5. Gertisser, R., Charbonnier, S., Keller, J., Quidelleur, X.: The geological evolution of Merapi volcano, Central Java. Indonesia. Bulletin Volcanology. **74**, 1213–1233 (2012). https://doi.org/10.1007/s00445-012-0591-3
6. Milsom, J., et al.: The Manokwari Trough and the western end of the New Guinea Trench. Tectonics. **11**(1), 145–153 (1992). https://doi.org/10.1029/91TC01257
7. Meilano, I., et al.: The 2021 mw 6.2 Mamuju, West Sulawesi, Indonesia earthquake: partial rupture of the Makassar Strait Thrust. Geophys. J. Int. **233**(3), 1694–1707 (2023). https://doi.org/10.1093/gji/ggac512
8. Gunawan, E., Kholil, M., Widyantoro, S.: Coseismic slip distribution of the 14 January 2021 Mamuju-Majene, Sulawesi, earthquake derived from GPS data. Nat. Hazards. **111**, 939–948 (2022). https://doi.org/10.1007/s11069-021-05084-y
9. Razi, P., et al.: 3D land mapping and land deformation monitoring using persistent scatterer interferometry (PSI) Alos PalSAR: validated by geodetic GPS and UAV. IEEE Access. **6**, 12395–12404 (2018). https://doi.org/10.1109/ACCESS.2018.2804899
10. Kausarian, H., Sri Sumantyo, J., Kuze, H., Aminuddin, J., Waqar, M.: Analysis of polarimetric decomposition, backscattering coefficient, and sample properties for identification and layer thickness estimation of silica sand distribution using I-band synthetic aperture radar. Can. J. Remote. Sens. **43**(2), 95–108 (2017). https://doi.org/10.1080/07038992.2017.1286935

11. Razi, P., et al.: 3D modeling using structure from motion technique for land observation in Kelok 9 flyover. J. Phys. Conf. Ser. **1876**(1) (2021). https://doi.org/10.1088/1742-6596/1876/1/012026
12. Widodo, J., et al.: Land subsidence rate analysis of Jakarta metropolitan region based on D-InSAR processing of sentinel data C-band frequency. J. Phys. Conf. Ser. **1185**(1), 012004 (2019). https://doi.org/10.1088/1742-6596/1185/1/012004
13. Widodo, J., et al.: Application of SAR interferometry using Alos-2 PALSAR-2 data as precise method to identify degraded peatland areas related to forest fire. Geosciences. **9**(11), 484 (2019). https://doi.org/10.3390/geosciences9110484
14. Aminuddin, J., Purbantoro, B., Lagrosas, N., Manago, N., Kuze, H.: Landsat-8 satellite and plan position indicator Lidar observations for retrieving aerosol optical properties in the lower troposphere. Adv. Remote Sens. **7**(03), 183 (2018). https://doi.org/10.4236/ars.2018.73013
15. Purbantoro, B., et al.: Comparison of aqua/terra modis and himawari-8 satellite data on cloud mask and cloud type classification using split window algorithm. Remote Sens. **11**(24), 2944 (2019). https://doi.org/10.3390/rs11242944
16. Aminuddin, J., Abdullatif, R.F., Anggraini, E.I., Gumelar, S.F., Rahmawati, A.: Development of convolutional neural network algorithm on ships detection in Natuna Islands-Indonesia using land look satellite imagery. Remote Sens. Appl.: Soc. Environ. **32**, 101025 (2023). https://doi.org/10.1016/j.rsase.2023.101025
17. Aminuddin, J., et al.: The LST and NDVI before and after earthquake of West Celebes 2021 using Terra/Aqua MODIS satellite image. In: International Conference of Geoscience and Remote Sensing Technology, pp. 105–113. Springer Nature Singapore, Singapore (2023) https://link.springer.com/chapter/10.1007/978-981-97-5746-6_9
18. Aminuddin, J., et al.: Derivation of atmospheric aerosol optical thickness by concurrent observation of sunphotometer and Himawari-8 satellite. In: International Conference of Geoscience and Remote Sensing Technology, pp. 93–103. Springer Nature Singapore, Singapore (2023) https://link.springer.com/chapter/10.1007/978-981-97-5746-6_8
19. Razi, P., Sumantyo, J., Febrianty, F., Nasucha, M., Aminuddin, J.: Interferometry synthetic aperture radar (InSAR) application for flood area detection observed by sentinel 1a. In: 2018 Progress in Electromagnetics Research Symposium (PIERS-Toyama), pp. 905–909. IEEE (2018). https://doi.org/10.23919/PIERS.2018.8598154
20. Fitrzyk, M., Engdahl, M., Fernandez, D.: Esa copernicus sentinel-1 exploitation activities. In: IGARSS 2019–2019 IEEE International Geoscience and Remote Sensing Symposium, pp. 5389–5392. IEEE (2019). https://doi.org/10.1109/IGARSS.2019.8898633
21. Rucci, A., Ferretti, A., Guarnieri, A., Rocca, F.: Sentinel 1 Sar interferometry applications: the outlook for sub millimeter measurements. Remote Sens. Environ. **120**, 156–163 (2012). https://doi.org/10.1016/j.rse.2011.09.030
22. Strozzi, T., et al.: Sentinel-1 Sar interferometry for surface deformation monitoring in low-land permafrost areas. Remote Sens. **10**(9), 1360 (2018). https://doi.org/10.3390/rs10091360
23. Rateb, A., Abotalib, A.: Inferencing the land subsidence in the Nile delta using sentinel-1 satellites and GPS between 2015 and 2019. Sci. Total Environ. **729**, 138868 (2020). https://doi.org/10.1016/j.scitotenv.2020.138868
24. Blasco, J.D., Foumelis, M., Stewart, C., Hooper, A.: Measuring urban subsidence in the Rome metropolitan area (Italy) with sentinel-1 snap-stamps persistent scatterer interferometry. Remote Sens. **11**(2), 129 (2019). https://doi.org/10.3390/rs11020129
25. Mancini, F., Grassi, F., Cenni, N.: A workflow based on snap–stamps open-source tools and GNSS data for psi-based ground deformation using dual-orbit sentinel-1 data: accuracy assessment with error propagation analysis. Remote Sens. **13**(4), 753 (2021). https://doi.org/10.3390/rs13040753

26. Weiß, T., Fincke, T.: Sensarp: a pipeline to pre-process sentinel-1 slc data by using esa snap sentinel-1 toolbox. J. Open Source Software. **7**(69), 3337 (2022). https://doi.org/10.21105/joss.03337
27. Rocca, F., Ferretti, A., Guarnieri, A., Prati, C.: InSAR processing: a mathematical approach. In: INSAR Principles, Guidelines for SAR Interferometry Processing and Interpretation, pp. C3–C29. ESA Publication (2007)
28. Braun, A., Veci, L.: Tops Interferometry Tutorial. ESA. Retrieved from https://step.esa.int/docs/tutorials/S1TBX%20TOPSAR%20Interferometry%20with%20Sentinel-1%20Tutorial_v2.pdf, Paris, France (2021)
29. Rees, G.: Physical Principles of Remote Sensing. Cambridge University Press (2013)
30. Rocca, F.: SAR interferometry applications: the outlook for sub millimeter measurements. In: 73rd EAGE Conference and Exhibition-Workshops 2011 cp-239-00008. European Association of Geoscientists & Engineers (2011). https://doi.org/10.3997/2214-4609.20144690
31. Wu, W., et al.: Quantifying the sensitivity of Sar and optical images three-level fusions in land cover classification to registration errors. Int. J. Appl. Earth Obs. Geoinf. **112**, 102868 (2022). https://doi.org/10.1016/j.jag.2022.102868
32. Anjasmara, I., Muthmainnah, N.: Analysis of the deformation of Madura island from SAR data processing using the DinSAR method. Geoid. **14**(1), 103–112 (2018). https://doi.org/10.12962/j24423998.v14i1.3952
33. Yu, H., Lan, Y., Yuan, Z., Xu, J., Lee, H.: Phase unwrapping in Insar: a review. IEEE Geosci. Remote Sens. Mag. **7**(1), 40–58 (2019). https://doi.org/10.1109/MGRS.2018.2873644
34. Razi, P., Sumantyo, J.T.S., Chua, M.Y., Ganefri, D.P., Tadono, T.: Monitoring of tectonic deformation in the seismic gap of the Mentawai Islands using ALOS-1 and ALOS-2. Remote Sens. Appl. **30**(December 2022), 100973 (2023). https://doi.org/10.1016/j.rsase.2023.100973
35. Supendi, P., Ramdhan, M., Priyobudi.: Foreshock–mainshock–aftershock sequence analysis of the 14 January 2021 (MW 6.2) Mamuju–Majene (West Sulawesi, Indonesia) earthquake. Earth Planets Space. **73**, 1–10 (2021). https://doi.org/10.1186/s40623-021-01436-x